Applied Physics Letters

Controlling the dopant profile for SRH suppression at low current densities in $\lambda \approx$ 1330 nm GaInAsP light-emitting diodes

Cite as: Appl. Phys. Lett. **116**, 203503 (2020); https://doi.org/10.1063/5.0002058
Submitted: 31 January 2020 . Accepted: 06 May 2020 . Published Online: 22 May 2020

Parthiban Santhanam, Wei Li, Bo Zhao, Chris Rogers, Dodd Joseph Gray, Phillip Jahelka, Harry A. Atwater, and Shanhui Fan

Applied Physics Letters ARTICLE scitation.org/journal/apl

Controlling the dopant profile for SRH suppression at low current densities in $\lambda \approx 1330$ nm GaInAsP light-emitting diodes

Cite as: Appl. Phys. Lett. **116**, 203503 (2020); doi: 10.1063/5.0002058
Submitted: 31 January 2020 · Accepted: 6 May 2020 ·
Published Online: 22 May 2020

Parthiban Santhanam,[1] Wei Li,[1] Bo Zhao,[1] Chris Rogers,[1] Dodd Joseph Gray, Jr.,[1] Phillip Jahelka,[2] Harry A. Atwater,[2] and Shanhui Fan[1,a)]

AFFILIATIONS

[1]Ginzton Laboratory, Department of Electrical Engineering, Stanford University, Stanford, California 94305, USA
[2]Thomas J. Watson Laboratories of Applied Physics, California Institute of Technology, Pasadena, California 91125, USA

[a)]Author to whom correspondence should be addressed: shanhui@stanford.edu

ABSTRACT

The quantum efficiency of double hetero-junction light-emitting diodes (LEDs) can be significantly enhanced at low current density by tailoring the spatial profile of dopants to suppress Shockley–Read–Hall recombination. To demonstrate this effect, we model, design, grow, fabricate, and test a GaInAsP LED ($\lambda \approx 1330$ nm) with an unconventional dopant profile. Compared against that of our control design, which is a conventional n^+-n-p^+ double hetero-junction LED, the dopant profile near the n-p^+ hetero-structure of the design displaces the built-in electric field in such a way that the J_{02} space charge recombination current is suppressed. The design principle generalizes to other material systems and could be applicable to efforts to observe and exploit electro-luminescent refrigeration at practical power densities.

As the solar photovoltaic and solid-state lighting industries have continued to deliver reductions in both the cost per semiconductor area and the cost per watt of their energy technology products,[1–5] the technology platforms which share capital base with them have become serious contenders for scalable energy technologies. Two of the most durable sources of demand for energy conversion that are yet to be "semiconductorized" are air conditioning and waste heat recovery. Both these demands have potentially viable solutions utilizing III–V optoelectronics.[6–11] However, it is also true that realizations of high-efficiency devices that can, in theory, meet these needs often carry the same stringent requirements on quantum efficiency as do Light-Emitting Diodes (LEDs) utilizing electro-luminescent cooling to act as refrigerators.

As a result, despite multiple recent demonstrations of photonic heat flux control capable of solid state cooling,[12–14] the pace of progress on these potential energy technologies has been limited by the technical challenges of fabricating devices with high enough quantum efficiencies for cooling at practical power densities. The general problem is twofold: first, electron–hole pairs injected into the luminescing material must be efficiently converted into photons within that material, and second, the photons thus generated must be able to escape the high refractive index typical of the luminescent materials that allow the first point to be satisfied.

Serious progress in overcoming both these challenges has been made experimentally in the past few years.[14–16] The light extraction efficiency challenge has been addressed in at least two distinct ways. First, a recent experiment redesigned LED structures[15] in the well-developed blue nitride LED material system for low current density where thinner current-spreading layers, which significantly reduce the probability that recycled photons will be lost to irreversible absorption in contact metal, can be sufficient. Second, but not less relevant, GaAs photo-diodes that served as photon-absorbing detectors were grown in series with GaAs emitters in the same epitaxial layer stack, thereby enabling direct light extraction from the LED to the photodetector, which is more efficient as compared to light extraction from an LED to free space.[14]

The other half of the technical challenge, to increase the fraction of injected electron–hole pairs which recombine radiatively (i.e., the Internal Quantum Efficiency or IQE to the light-emitter community; alternatively the Internal Radiative Efficiency or IRE to the photo-voltaic community), has recently been approached by attempts to suppress parasitic Shockley–Read–Hall (SRH) recombination that prevents cooling from being observed at lower forward bias voltages, where the problem of light extraction is more forgiving. Operating an LED at a slightly lower forward bias voltage than typical results in a larger ratio between the so-called photon voltage $V_p \equiv \frac{\hbar\omega}{q}$, where $\hbar\omega$ is the emitted photon's

energy and q is the charge of an electron, with the applied voltage V. When the ratio V_p/V is greater than unity but by a small margin, as tends to be the case in blue nitride LEDs, the margin for error is correspondingly small. A ratio of $V_p/V = 1.03$, for instance, implies that not more than 3% of the internally generated photons may be lost to parasitic absorbing structures (e.g., contacts) without entirely eliminating the possibility of net cooling. A ratio of $V_p/V = 1.30$ increases this margin for error tenfold, making experimental realization drastically more tractable. This approach makes the observation of an emitter with a large steady-state temperature reduction less demanding and could enable photonic solid state coolers that support large temperature differences with very small cold-side heat loads.

Recent work has produced a near-infrared LED with suppressed SRH recombination at the values of V_p/V most relevant to electroluminescent cooling.[16] In Ref. 16, the authors designed, fabricated, and tested an LED that made use of the spectacularly low interfacial surface recombination velocity at the hetero-interface between the luminescent material (1.3 eV-GaInAs) and the wider bandgap carrier confining material (GaInP) to extend the high IQE of near-infrared LEDs to much lower current densities where parasitic SRH recombination is usually dominant. The structure in Ref. 16 utilizes a GaInAs quantum well to confine the injected carriers to a thin layer in which they experience SRH recombination a very small fraction of time. Thus, they observe very high IQE from their LEDs even at forward biases $\approx$ 200 mV below the emitted photon energy. This strategy for increased IQE, however, comes at the price of current density as only electron-hole pairs in the same narrow interval can contribute to radiative recombination. As a result, the current density achieved in Ref. 16 is more than two orders of magnitude below the detailed balance limit for an opaque body of the same bandgap. In pursuit of higher current densities at the same voltage, some of this may be addressed by the use of multiple quantum wells or much thicker emitting layers, but whether such structures can maintain high IQE remains to be seen.

In this work, we aimed to improve IQE at deep sub-bandgap bias voltages through a distinct SRH suppression strategy, alluded to but not fully examined in Ref. 19, which utilizes a micrometer-thick emitting layer so that even in a device realization with near-complete SRH suppression, the diode remains near the detailed balance limit for current density. We report work on GaInAsP LEDs, grown lattice-matched to InP substrates and emitting photons at a free-space wavelength of $\lambda \approx 1330$ nm, whose epitaxial layer stack design aims to extend downward the range of voltages where high IQE is observed by the suppression of bulk non-radiative SRH recombination. We subsequently fabricate devices resembling Fig. 1(a) and characterize them. Our approach targets the bulk SRH recombination in the electrically non-neutral space charge region around the p-n junction (i.e., the often-parasitic J_{02} current[20] contribution that causes the J–V curve to exhibit a diode ideality factor of 2) of a near-infrared LED with a micrometer-thick emitting layer. It does so in a way that is readily generalized to other promising material systems including GaAs.

The technique presented here bears some relevance to the ongoing discussion in the GaAs photovoltaic (PV) research community of measurements[21,22] indicating significant suppression of device-integrated bulk SRH recombination from the use of a "thick" emitter layer. While our work also aims to suppress device-integrated SRH recombination in a similar voltage regime, in those works, the depletion regions of the PV cells fall entirely in the GaAs absorber layers in all emitter configurations considered. Thus, while those SRH suppression effects may arise from differences in the diffusion length or mobility across the p–n junction, no bandgap difference is present to change the intrinsic carrier concentration across it. Since the effect presented here is distinct, both mechanisms may ultimately prove to be useful together in future designs of both LEDs and PV cells.

By inserting one higher-doped layer into n-GaInAsP and one lower-doped layer into the p-InP regions directly surrounding the p–n junction, most of the bulk SRH can, in theory, be displaced enough to place its peak in the wider bandgap material. As we show presently, the aggregate rate at which carriers undergo bulk SRH recombination integrated over the volume of the device is thereby reduced by several orders of magnitude.

The epitaxial layer stack designs on which the experiments in this Letter are based are shown in Table I with the layers modified to achieve SRH suppression in bold. Design $\mathcal{A}$ includes the proposed suppression layers, while Design $\mathcal{B}$ serves as a control against which to evaluate $\mathcal{A}$.

To explain the design process and clarify the intended generalization of the design principle into other material systems, we focus on the electron transport in the region surrounding the p–n hetero-

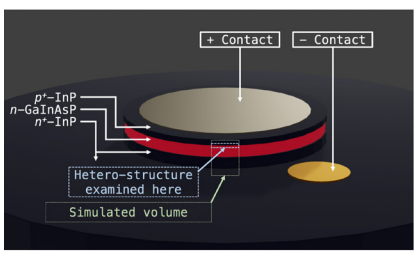

(a) Graphical depiction.

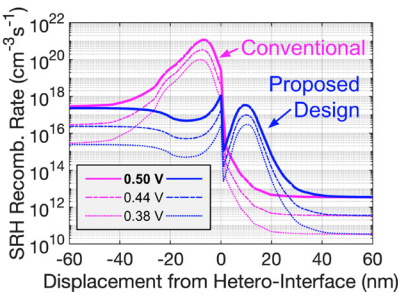

(b) SRH profiles.

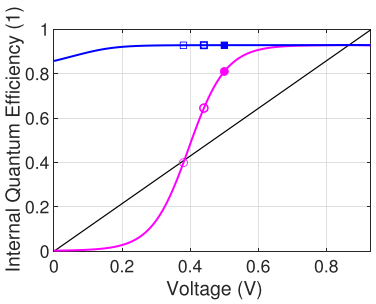

(c) Low-voltage IQE enhancement.

FIG. 1. In (a), a depiction of the fabricated devices, which highlights the n-p^+ hetero-structure examined here. In (b), the modeled spatial distribution of bulk trap-assisted SRH recombination is shown to have its peak displaced between the conventional design (magenta) and the design for SRH suppression (blue). The solid lines correspond to 500 mV of forward bias, while the dashed-dotted and dotted lines represent the same devices at 60 and 120 mV of lower bias, respectively. Negative displacements from the hetero-interface are in n-GaInAsP. In both semiconductors, we have taken $\tau_p = 3\mu$s and $\tau_n = 10$ ns.[17,18] In (c), the consequences of the design change for IQE are plotted vs voltage. The straight diagonal line is the minimum IQE for which refrigeration is possible for ideal photon extraction. (a) Graphical depiction. (b) SRH profiles. (c) Low-voltage IQE enhancement.

TABLE I. Epitaxial layer stacks as designed prior to growth. Design $\mathcal{A}$ is a modified double hetero-junction layer stack, which utilizes an inhomogeneous doping profile to displace the depletion region out of the GaInAsP and into the adjacent InP layer. Design $\mathcal{B}$ serves as a control. The layers modified to achieve SRH suppression are shown in bold.

Thickness (nm)	Material	Doping in $\mathcal{A}$ $\lvert N_D - N_A\rvert$ (cm^{-3})	Doping in $\mathcal{B}$ $\lvert N_D - N_A\rvert$ (cm^{-3})
480	p-InP	1×10^{18}	1×10^{18}
20	p-InP	$\mathbf{1 \times 10^{17}}$	$\mathbf{1 \times 10^{18}}$
20	n-GaInAsP	$\mathbf{2.26 \times 10^{18}}$	$\mathbf{4 \times 10^{17}}$
980	n-GaInAsP	4×10^{17}	4×10^{17}
50	n-InP	4×10^{17}	4×10^{17}
1250	n-InP	2×10^{18}	2×10^{18}
200	n-InP	1×10^{18}	1×10^{18}
$\approx 370\mu$m	i-InP	Semi-Insulating	Semi-Insulating

junction buried 500 nm below the surface in each design (i.e., where the two designs differ). We seek to model the transport here for a forward bias voltage V below the bandgap energy's voltage scale E_{gap}/q by several multiples of the thermal voltage. This range of voltages has been previously referred to[23] as the "deep sub-bandgap" bias regime and is tens to hundreds of milli-volts below the bias voltages where LEDs are typically designed to operate. At these deep sub-bandgap operating points, a very significant fraction of the current flowing through the device is lost to trap-assisted SRH recombination.

Furthermore, the standard formulation of SRH recombination indicates that in an epitaxially grown p–n diode, the spatial distribution of bulk SRH recombination is highly localized around a particular plane normal to the growth direction. In this Letter, we refer to this plane as the active trap plane. Here, we have used the standard formulation[20,24,25] for the local rate of trap-assisted Shockley–Read–Hall (SRH) recombination as expressed by the following equation:

$$W_{\mathrm{SRH}} = \frac{\left(e^{\frac{qV}{k_B T}} - 1\right) \cdot n_i^2}{(n + n_i)\tau_p + (p + n_i)\tau_n} \quad . \tag{1}$$

The above equation assumes that the trap spectrum is a delta function and nonzero only at the intrinsic Fermi level of each semiconductor. If we further assume that the SRH lifetimes of the electrons and holes are equal (i.e., $\tau_n = \tau_p = \tau$), unlike in the simulations behind Figs. 1(b) and 1(c) for which lifetimes can be found in the caption, we may further simplify the denominator of Eq. (1) to find that

$$W_{\mathrm{SRH}}(z) \propto \frac{1}{n(z) + p(z) + 2n_i(z)} \quad . \tag{2}$$

Since n and p are varying in z and away from the hetero-junction itself that variation is monotonic, if we temporarily assume that the removed parts of Eq. (1) are not varying spatially, we should expect a local maximum to $W_{\mathrm{SRH}}(z)$ around the plane where $n + p$ is minimized. Since in quasi-equilibrium, the product of the electron and hole concentrations np is fixed for a fixed Fermi level separation, this minimum is located where $n = p$.

Figure 1(b) depicts the results of numerical simulations conducted using the commercial electron transport CHARGE solver within Lumerical Device.[26] The net recombination rate per unit volume around the hetero-interface nearest the active trap plane for Design $\mathcal{A}$ is shown alongside that for Design $\mathcal{B}$. Design $\mathcal{B}$ (shown in magenta) has its SRH rate peak ≈ 7 nm from the hetero-interface into n-GaInAsP. The qualitatively similar local maximum in the SRH rate of Design $\mathcal{A}$ (shown in blue) falls 10 nm away from the hetero-interface into the wide-bandgap p^+-InP. We note that the global maximum of the volumetric SRH rate in our simulation of Design $\mathcal{A}$ is in fact at the exact grid point of the hetero-interface. However, our discussion will not focus on this plane but instead that of the local maximum 10 nm away.

Due to the strength of the built-in electric field in this region and our assumptions about the trap spectrum, this local maximum is fairly sharp. At low voltages, a field strength on the order of 10^7 V/m is typical. In this case, we may use the room temperature rule of thumb of 60 meV/decade for the exponential decay of the concentration of electrons and holes as a function of energy in the Boltzmann limit at $\approx$ 300 K to quantify this sharpness. For the assumed field strength, a plane just 6 nm away from the active trap plane would necessarily have one of either n or p, a full $10\times$ larger than that at the SRH local maximum. Since both n and p enter the denominator additively in Eq. (2), this indicates that $\approx$ 99% of the integrated recombination takes place within a 25 nm window. For the admittedly unphysical case of a delta function trap spectrum, more than half of the recombination falls inside a window of width 50 Å.

Temporarily neglecting the additional complication of the hetero-junction, the physical interpretation of this peak is reasonably simple. Outside of this window, we find that the traps are less active. If we consider planes displaced in the growth direction toward the n layers, we find that the hole concentration p is too low there, and so the SRH process is bottlenecked by slow hole capture rates. Similarly, in planes displaced in the growth direction toward the p terminal of the device, we find that the electron concentration n is too low and the SRH process is bottlenecked by slow electron capture rates.

For our control structure in Design $\mathcal{B}$, this peak falls within the narrow bandgap GaInAsP active region. Our goal in Design $\mathcal{A}$ is to displace this spatial peak in the SRH rate into the wider gap InP material so that the n_i^2 term in the numerator of Eq. (1) can suppress it. To do this, we will modify the dopant impurity profile from that in Design $\mathcal{B}$ to that in Design $\mathcal{A}$, as shown in Table I.

Custom epitaxial growths were purchased commercially from OEpic, Inc. in Sunnyvale, CA. Growth was done by MOCVD on Fe-doped semi-insulating InP substrates. The growth processes reported here were all done during a pair of back-to-back runs of the same reactor with the intention of eventually comparing device characteristics in a controlled manner. The target alloy for the 1 μm-thick quaternary in both growth processes was $Ga_xIn_{1-x}As_{1-y}P_y$ with $y \approx 0.33$ and x taken to retain lattice matching to InP. However, the compositions (i.e., x and y) of the alloy were not measured directly.

The first set of experiments done to verify that the films had been grown as intended was Photo-Luminescence (PL) measurements on bare epitaxy. Room temperature PL measurements are shown in subfigure (b) of Fig. 3. Cryogenic PL measurements (performed on samples that had undergone a mesa etch but no further processing) were taken in a chamber cooled by liquid helium, but due to poor heat sinking in the sample mounting solution, the exact temperature of the sample was highly uncertain. The primary conclusion of the PL experiments was that the devices fabricated from

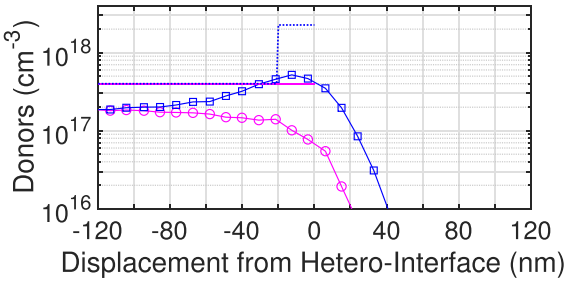

FIG. 2. SIMS was used to investigate the unprocessed epitaxy. The discrete markers denote experimental data, while the marker-free lines represent the design dopant profile. As in previous figures, blue denotes $\mathcal{A}$ and magenta denotes $\mathcal{B}$.

this epitaxy should emit light with a free space wavelength of around $\lambda \approx 1330$ nm.

The second set of experiments was aimed at verifying the distinction between the films grown to meet the two different design specifications. Secondary Ion Mass Spectrometry (SIMS) analysis was done by Evans Analytical Group. The primary conclusion drawn from the SIMS data shown in Fig. 2 was that the realized silicon donor concentration in the emitting-bandgap SRH suppression layer was significantly higher than that in the corresponding layer of the control sample, but was far short of the design concentration. One would expect this to create a much smaller change in the IQE of resulting LEDs than that shown in Fig. 1(c). As shown in Fig. 2, the additional silicon donors detected by SIMS were localized to a region ≈60 nm thick rather than 20 nm as in the design. Moreover, the z-integrated density of silicon in the sample grown targeting Design $\mathcal{A}$ exceeded that of the sample grown targeting Design $\mathcal{B}$ by $\approx 1.8 \times 10^{12}\,\mathrm{cm}^{-2}$, which is lower than the extra donor density of $\approx 3.7 \times 10^{12}\,\mathrm{cm}^{-2}$ as designed. Unfortunately, neither the acceptor concentrations nor the ionization fraction of the silicon dopants has yet been measured directly in any part of the epitaxial films.

LEDs were fabricated from these films. We used the lithography capabilities of the Stanford Nanofabrication Facility and the Stanford Nano Shared Facilities, with particular reliance on the Heidelberg Maskless Aligner MLA150, Shipley S1813 photo-resist, and Metal-Free developer MF319. All masks were designed manually with Python scripts used to generate CIF files. Etching was done by a combination of 3:1 H_3PO_4:HCl, which selectively etched InP, and 1:1:10 H_2O:H_2O_2:H_2SO_4, which selectively etched GaInAsP. The contacts were formed by lift-off processes, which utilized the same resist as for the etch patterns, and a pair of deposition tools. n-type contacts were Ti/Pt/Au deposited using electron beam evaporation. p-type contacts were annealed Pd/Zn/Pd. Prior to the p-metal contacts reported here, a generation of devices was made using Ti/Pt/Au for both contacts; the absence of an epitaxial contact layer resulted in Schottky barriers, which prohibited meaningful I–V and L–I characterization.

Two types of diode structures were fabricated and tested. Small circular mesa type diodes with an active emitting area of 0.1 mm^2 each were designed for high current density. Larger square mesa diodes were designed for lower current density measurements, each having an active emitting area of 8 mm^2.

The current–voltage and light–current characteristics of the devices were measured. Imperfections in various stages of the fabrication process led to some variation in device behavior both within a given die and from die-to-die. Particularly common were parasitic shunts presumed to arise from flashes of contact metal unintentionally attached to the sidewalls of the devices amid the lift-off contact fabrication process.

Experiments were performed near room temperature, measured at about 295 K. The fabricated diodes were placed in a variety of geometries near a 1 cm^2 ThorLabs FDG10X10 large-area free-space germanium photo-diode as well as a smaller ThorLabs FDG05 germanium photo-diode of 5 mm diameter. The photo-currents from these detectors were then amplified by a ThorLabs PDA200C TIA to measure their electro-luminescence signals. Initially, the LED-detector interface

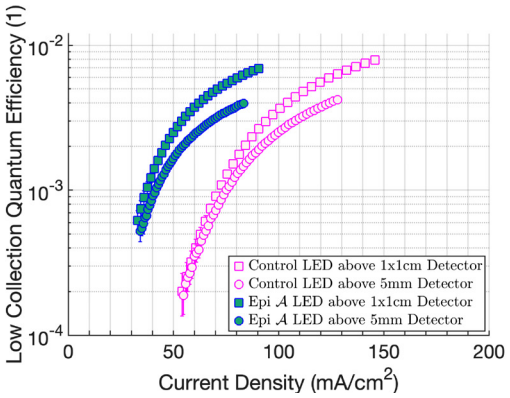

(a) Quantum Efficiency at Photo-Detector.

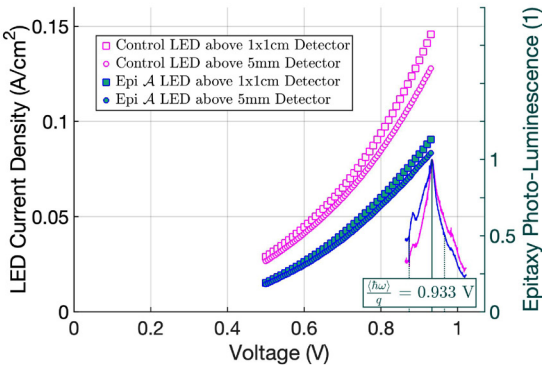

(b) Device J-V and Epitaxy PL.

FIG. 3. Two 8 mm^2 LEDs were placed about 1 mm above each of the two photodetectors. The detectors' collection efficiency was reduced by this choice of spacing, but effects from inconsistent optical coupling between the emitter and the detector were thereby removed. In (a), "Low Collection Quantum Efficiency" (i.e., detector's photo-current divided by the LED current, interpreted as a measure of the true quantum efficiency multiplied by some unknown low collection efficiency) is shown vs current density. Solid blue markers denote Design $\mathcal{A}$; empty magenta markers denote Design $\mathcal{B}$. In (b), the J-V data are plotted alongside the relative intensity PL spectra from the epitaxial structures corresponding to their color. The label "Epitaxy Photoluminescence" is used to distinguish the shown spectrum from a PL spectrum of a fully fabricated device. (a) Quantum efficiency at the photo-detector. (b) Device J-V and epitaxy PL.

showed limited repeatability. We ascribe this observation to dust and other debris, a hypothesis supported by an appropriately significant increase in the signal seen when high-index immersion oil was used. For repeatability, the measurements were taken when the emitting diode chips were placed atop a nylon washer at a height about 1 mm above the photo-sensitive surface of each of the two detectors described above. We hypothesize that the difference in the current range of measurements arises from temperature variation. Devices were probed manually in a station with shielded electrical connections to a Keithley 2635B Sourcemeter.

Figure 3 presents data taken on the large 8 mm^2 diodes at voltages ranging from 500 mV to 920 mV. The figure shows that the epitaxial layer stack design changes from Design $\mathcal{B}$ to Design $\mathcal{A}$ resulted in less current leaking through the device as intended. The decrease in current for a given quantum efficiency is found to be $\approx 2\times$. This indicates moderate suppression of non-radiative recombination at low current density.

Finally, simulations were conducted incorporating the measured SIMS donor profiles. When the remainder of the structure was assumed to be identical, the corresponding decrease in current was $\approx 3.6\times$ at the same quantum efficiency as above with estimated detector collection, indicating that about 3/4 of the SRH current was suppressed. When the simulated acceptor profile exactly matched with that shown in Table I, a current ratio $>10^4\times$ was found, indicating that an ideal acceptor profile along with donors from SIMS data gave nearly the full effect as designed.

The experiments reported here provide significant evidence that rational design of the dopant profile of a near-infrared LED represents a viable technical de-risking pathway for the development of energy conversion devices that exhibit net refrigeration at bias voltages $\frac{1}{2}(E_{gap}/q) < V < (E_{gap}/q - 3k_BT)$.

Dr. Ping-Show Wong of OEpic performed the metalorganic chemical vapor deposition (MOCVD) epitaxial growth. Room temperature PL spectra were acquired in collaboration with Dr. Tomás Sarmiento in the lab of Professor Jelena Vuckovic. Tom Carver deposited the *n*-metal Ti/Pt/Au. Dr. Michelle Sherrott helped diagnose an early *p*-metal issue. Professor Eric Pop provided advice and aid in characterization facilities access. The selective wet etch recipes were based on suggestions from Dr. Vijay Jayaraman of Praevium Research, Inc. This work was supported by the U.S. Department of Energy (DoE) "Light-Material Interactions in Energy Conversion" Energy Frontier Research Center (EFRC) under Grant No. DE-SC0001293 and the U.S. DoE "Photonics at Thermodynamic Limits" EFRC under Grant No. DE-SC0019140.

DATA AVAILABILITY

The data that support the findings of this study are available from the corresponding author upon reasonable request.

REFERENCES

[1]J. Trube, M. Fischer, G. Erfert, C.-C. Li, P. Ni, M. Woodhouse, P. Li, A. Metz, I. Saha, R. Chen, and Q. Wang, "International technology roadmap for photovoltaics (ITRPV)," Industry Sponsored report (Steering committee of the ITRPV, 2019).
[2]R. Haitz, F. Kish, J. Tsao, and J. Nelson, "The case for a national research program on semiconductor lighting," Report No. SAND2000-1612 (Sandia National Laboratories, Albuquerque, New Mexico/Livermore, California, 2000).
[3]R. V. Steele, "The story of a new light source," Nat. Photonics **1**, 25 (2007). Focus.
[4]R. Haitz and J. Y. Tsao, "Solid-state lighting: 'The case' 10 years after and future prospects," Phys. Status Solidi A **208**, 17–29 (2011).
[5]B. F. Gerke, A. T. Ngo, and K. S. Fisseha, "Recent price trends and learning curves for household LED lamps from a regression analysis of Internet retail data," "DOE Report No. LBNL-184075," (US Department of Energy, LBNL, EERE Division, 2015).
[6]T. P. Xiao, K. Chen, P. Santhanam, S. Fan, and E. Yablonovitch, "Practical efficiency limits of electroluminescent cooling," Proc. SPIE **10936**, 109360B (2019).
[7]O. Heikkila, J. Oksanen, and J. Tulkki, "Ultimate limit and temperature dependency of light-emitting diode efficiency," J. Appl. Phys. **105**, 093119 (2009).
[8]J. Piprek and Z.-M. Li, "Electroluminescent cooling mechanism in InGaN/GaN light-emitting diodes," Opt. Quantum Electron. **48**, 72 (2016).
[9]K. Chen, T. P. Xiao, P. Santhanam, E. Yablonovitch, and S. Fan, "High-performance near-field electroluminescent refrigeration device consisting of a GaAs light emitting diode and a Si photovoltaic cell," J. Appl. Phys. **122**, 143104 (2017).
[10]N.-P. Harder and M. A. Green, "Thermophotonics," Semicond. Sci. Technol. **18**, S270 (2003).
[11]B. Zhao, P. Santhanam, K. Chen, S. Buddhiraju, and S. Fan, "Near-field thermophotonic systems for low-grade waste-heat recovery," Nano Lett. **18**, 5224–5230 (2018).
[12]M. P. Hehlen, J. Meng, A. R. Albrecht, E. R. Lee, A. Gragossian, S. P. Love, C. E. Hamilton, R. I. Epstein, and M. Sheik-Bahae, "First demonstration of an all-solid-state optical cryocooler," Light: Sci. Appl. **7**, 15 (2018).
[13]L. Zhu, A. Fiorino, D. Thompson, R. Mittapally, E. Meyhofer, and P. Reddy, "Near-field photonic cooling through control of the chemical potential of photons," Nature **566**, 239–244 (2019).
[14]I. Radevici, J. Tiira, T. Sadi, S. Ranta, A. Tukiainen, M. Guina, and J. Oksanen, "Thermophotonic cooling in GaAs based light emitters," Appl. Phys. Lett. **114**, 051101 (2019).
[15]L. Y. Kuritzky, A. C. Espenlaub, B. P. Yonkee, C. D. Pynn, S. P. DenBaars, S. Nakamura, C. Weisbuch, and J. S. Speck, "High wall-plug efficiency blue III-Nitride LEDs designed for low current density operation," Opt. Express **25**, 30696 (2017).
[16]N. Li, K. Han, W. Spratt, S. Bedell, J. Ott, M. Hopstaken, F. Libsch, Q. Li, and D. Sadana, "Ultra-low-power sub-photon-voltage high-efficiency light emitting diodes," Nat. Photonics **13**, 588–592 (2019).
[17]See http://www.ioffe.ru/SVA/NSM/Semicond/InP/electric.html for information about low-injection SRH lifetimes in InP.
[18]Y. Rosenwaks, B. R. Thacker, A. J. Nozik, Y. Shapira, and D. Huppert, "Recombination dynamics at Inp/liquid interfaces," J. Phys. Chem. **97**, 10421–10429 (1993).
[19]D. J. Gray, Jr., P. Santhanam, and R. J. Ram, "Design for thermo-electric pumping in light-emitting diodes," Appl. Phys. Lett. **103**, 123503 (2013).
[20]A. S. Grove, *Physics and Technology of Semiconductor Devices* (John Wiley & Sons, Inc., 1967).
[21]M. P. Lumb, M. A. Steiner, J. F. Geisz, and R. J. Walters, "Incorporating photon recycling into the analytical drift-diffusion model of high efficiency solar cells," J. Appl. Phys. **116**, 194504 (2014).
[22]G. Bauhuis, P. Mulder, Y.-Y. Hu, and J. Schermer, "Deep junction III–V solar cells with enhanced performance," Phys. Status Solidi A **213**, 2216 (2016).
[23]P. Santhanam, "Electro-luminescent cooling in the deep sub-bandgap bias regime," Proc. SPIE **9000**, 900007 (2014).
[24]R. N. Hall, "Electron-hole recombination in germanium," Phys. Rev. **87**, 387 (1952).
[25]W. Shockley and W. T. Read, Jr., "Statistics of the recombinations of holes and electrons," Phys. Rev. **87**, 835–842 (1952).
[26]See https://www.lumerical.com/products/ for information about the CHARGE transport solver within Lumerical Device.